

# Geometric quench and non-equilibrium dynamics of fractional quantum Hall states

Zhao Liu,<sup>1</sup> Andrey Gromov,<sup>2</sup> and Zlatko Papić<sup>3</sup>

<sup>1</sup>*Freie Universität Berlin, Dahlem Center for Complex Quantum Systems  
and Institut für Theoretische Physik, Arnimallee 14, 14195 Berlin, Germany*

<sup>2</sup>*Kadanoff Center for Theoretical Physics, University of Chicago, Illinois 60637, USA*

<sup>3</sup>*School of Physics and Astronomy, University of Leeds, Leeds LS2 9JT, UK*

(Dated: May 9, 2022)

We introduce a quench of the geometry of Landau level orbitals as a probe of non-equilibrium dynamics of fractional quantum Hall states. The quench protocol can be experimentally implemented as a sudden tilt of the magnetic field. Using the recently developed bimetric theory of fractional quantum Hall states, we describe the post-quench dynamics as due to oscillations of a single collective degree of freedom – the emergent spin-2 graviton mode, which is the long wavelength limit of the Girvin-MacDonald-Platzman magnetoroton mode. The predictions of bimetric theory are confirmed by exact numerical simulations of the dynamics at short times. In addition to the spin-2 mode, we demonstrate that fractional quantum Hall states host a tower of higher-spin collective modes, which can be studied using the geometric quench. Our results lay the foundation for the exploration of geometry and dynamics out of equilibrium in strongly correlated phases of matter in two spatial dimensions.

PACS numbers: 73.43.Lp, 71.10.Pm

## I. INTRODUCTION

Fractional quantum Hall (FQH) states are an epitome of topological phases of matter, featuring exotic phenomena such as fractionalization [1], topological order [2], and protected edge excitations [3, 4]. These phenomena often arise as emergent properties of a two-dimensional (2D) electron system in a perpendicular magnetic field [5]. As a consequence of Landau level quantization in strong magnetic fields, electrons in these systems have negligible kinetic energy, which paves the way for Coulomb interaction to produce a variety of exotic effects, whose experimental hallmark is the fractional quantization of the Hall conductance [6]. The strong, on-going interest in FQH phases is fueled, on the one hand, by the motivation to understand the non-perturbative physics of strongly-correlated systems, while on the other hand, the unique features of quasiparticles in such systems might allow to store and manipulate quantum information in technological devices that are robust to many sources of error [7].

Given the intricate, purely interacting nature of FQH states, it comes as no surprise that the existing research mainly focused on their equilibrium (static) properties at zero temperature. These properties have often been described using two closely related frameworks: trial wave functions [1, 8–10] and topological quantum field theory (TQFT) [11], which encode the linear response functions [12, 13], exotic quasiparticles (“anyons”) [14, 15] characterized by the fractional charge, spin and statistics [16], robust edge modes [4] and the topological degeneracy on a torus [2, 17]. The predictions of microscopic trial states and TQFT have been tested in numerical simulations of unprecedented accuracy, in particular in the case of Laughlin [1, 18] and composite fermion states [19].

Besides low-energy properties, the complete under-

standing of a quantum system requires the understanding of its *dynamics*, which is determined by the system’s excited states, possibly at high energy densities. This dynamics can be physically probed using the global quantum quench: prepare the system in its ground state  $|\psi_0\rangle$ ; abruptly change the Hamiltonian,  $H \rightarrow H'$ ; let the system evolve and perform measurements on the time-evolved state. For systems which are intrinsically decoupled from the environment, this quench amounts to the innocuous-looking Schrödinger evolution,  $|\psi(t)\rangle = \exp(-iH't)|\psi_0\rangle$ , where  $|\psi_0\rangle$ , crucially, is *not* an eigenstate of the quench Hamiltonian,  $H'$ . Even though Schrödinger evolution can be written in such a compact way, it can nevertheless lead to incredibly complex outcomes as it might involve arbitrary highly excited eigenstates of  $H'$ . In one-dimensional integrable systems, where such eigenstates can be computed using techniques like algebraic Bethe ansatz, a particularly deep theoretical understanding of quenches has been achieved (see the recent review [20]) and verified in cold atom experiments [21]. Other notable examples include one-dimensional critical systems where conformal invariance allows to analytically describe the post-quench dynamics of various observables (see Ref. [22] and references therein) and their holographic duals [23], where quantum quench is interpreted as a process of black hole formation and decay.

In this work we introduce a new type of *geometric quench* and use it to study dynamics of FQH states out of equilibrium. While in integrable systems the term “geometric quench” refers to a sudden change of the size of system [24–27] (e.g., controlled by the trap potential in cold atomic systems), our setup assumes that the size of the system remains fixed, but the effective mass tensor of particles undergoes an abrupt change. This way of probing the system is quite physical. Indeed, changing the

effective mass tensor can be achieved directly by tilting the magnetic field, i.e., by introducing a component of magnetic field tangential to the plane occupied by particles. This technique is regularly employed in FQH experiments to measure spin polarization of various states [28], while in a more recent generation of experiments it has been used to map out the anisotropy of the composite fermion Fermi surface [29].

Geometric quench is designed to excite the neutral degrees of freedom of FQH states, which have certain universal features that are geometric in nature. Two major examples are the geometric response function known as Hall viscosity [30–32] and the geometric degrees of freedom responsible for the nematic transition [33, 34]. The former can be understood in terms of response to the variations of ambient geometry [13, 35–42], while the latter can be formulated as fluctuating geometry [43, 44] (see also Ref. [45] for a related perspective). We will show that the real-time dynamics following the geometric quench is accurately described by the excitations of geometric degrees of freedom that characterize the underlying FQH states [43]. More specifically, in the case of Laughlin states, the (weak) geometric quench excites a single degree of freedom of angular momentum (or spin)  $L = 2$  described by a fluctuating, “intrinsic metric” [46]. This spin-2 degree of freedom is described by a symmetric matrix, which makes it formally similar to the fluctuating space-time metric — a variable that one would like to use in a theory of quantum gravity. For the lack of a better term we will continue to refer to this geometric degree of freedom as “graviton” [47, 48]. The geometric quench thus allows to excite the emergent FQH graviton and to observe its non-trivial dynamics in time. One has to bear in mind that the graviton discussed below is non-relativistic and massive (i.e., gapped). The closest relativistic relative of the geometric aspects of the FQH problem is the zwei-dreibein theory of 3D massive gravity [49] (see also Ref. [50]).

In order to model the geometric quench, we utilize two recent advances in the theory of the FQH effect: the formulation of bimetric theory [44, 51], which describes topological properties of FQH states on curved surfaces whilst incorporating the mentioned spin-2 excitation, and the generalization of Haldane pseudopotentials [52] to systems with broken rotational invariance. Bootstrapping these methods, we derive the analytic description of the real-time dynamics of FQH states following a geometric quench, and confirm it against numerical simulations for the case of Laughlin states. Our main findings are: (i) bimetric theory is generalized to the case of anisotropic systems, and used to derive the system of coupled *non-linear* differential equations [Eqs. (10) and (11)] that describe the dynamics of a FQH state following the quench; (ii) when the quench is sufficiently weak, the non-linear, post-quench equations of motion can be linearized and thereby admit a simple solution in the form of harmonic oscillation; (iii) we demonstrate that the oscillation is caused by the excited states with quadrupolar order (i.e.,

spin-2) in the continuum of the spectrum, whose energy gives an independent confirmation of the oscillation frequency; (iv) the predictions of bimetric theory are in *full* agreement with exact diagonalization of finite systems at short times, and generally capture well the oscillations in the dynamics at moderate times; (v) we demonstrate that the exact dynamics can be accurately approximated by an exponentially small fraction of all states in the Hilbert space, further confirming the bimetric picture. Based on these results, we also consider some generalizations such as more realistic (non-instantaneous) quenches and quenches that excite putative higher-spin modes in the spectrum. The latter are not captured by bimetric theory and suggest a much richer *higher-spin* structure in the FQH states, in particular calling for an extension of the geometric picture of Laughlin states [43].

The remainder of the paper is organized as follows. In Sec. II we provide further details about the quench setup and the physical motivation behind it. In Sec. III we use bimetric theory to derive the post-quench dynamics. In Sec. IV we introduce our numerical method, and show that generalized pseudopotentials allow to independently verify the frequency of the post-quench dynamics. Sec. V contains the bulk of our numerical results and detailed comparisons against theory. Sec. VI provides an example of a quench that excites higher-spin modes in the spectrum, which currently do not have a theoretical description. Our conclusions are presented in Sec. VII, while the Appendices contain additional data and extensions of our results.

## II. GEOMETRIC QUENCH OF A FRACTIONAL QUANTUM HALL STATE

The Hamiltonian describing a FQH system is given by [5]

$$H = \frac{1}{N_\Phi} \sum_{\mathbf{q}} \bar{V}_{\mathbf{q}} \bar{\rho}_{\mathbf{q}} \bar{\rho}_{-\mathbf{q}}, \quad (1)$$

where the sum runs over the 2D Brillouin zone (threaded by  $N_\Phi$  flux quanta) and  $\bar{\rho}_{\mathbf{q}} = \sum_{j=1}^N e^{i\mathbf{q}\cdot\mathbf{R}_j}$  is the density operator projected to a single Landau level (LL). The projection to a LL imposes the non-commutative geometry of the “guiding center coordinates”,  $[R_i^a, R_j^b] = -i\ell_B^2 \epsilon^{ab} \delta_{i,j}$ , where  $\ell_B = \sqrt{\hbar/eB}$  is the magnetic length [5]. This non-trivial constraint, along with the absence of kinetic energy in Eq. (1), is sufficient to give rise to a wide variety of ordered phases, depending on the filling factor,  $\nu = N/N_\Phi$  and the details of the (projected) interaction potential,  $\bar{V}_{\mathbf{q}}$ . Note that because the guiding centers do not commute, bosonic FQH states are also possible and realize a similar variety of phases [53, 54]. In this paper, we focus on the simplest Laughlin states, which occur at filling  $\nu = 1/2$  for bosons and  $\nu = 1/3$  for fermions.

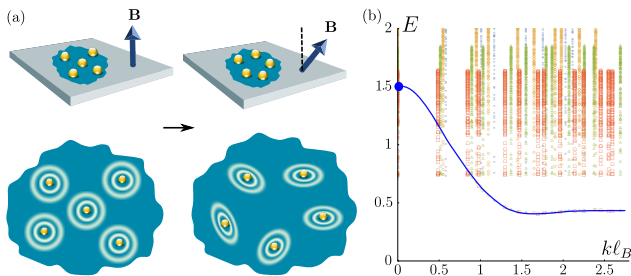


FIG. 1. (a) Geometric quench protocol: instantaneous tilt of the magnetic field induces dynamics of the intrinsic metric, which describes the shape of particle-flux composites that form a FQH state. (b) The excitation spectrum of the  $\nu = 1/3$  Laughlin state, obtained by exact diagonalization of its  $V_1$  parent Hamiltonian, in systems with  $N = 7 - 10$  electrons. Blue line traces out the SMA collective mode [55], which transforms into an emergent graviton excitation in the  $k \rightarrow 0$  limit (around energy  $E \approx 1.5$ ). It will be shown in Sec. III that geometric quench induces oscillatory dynamics of the graviton mode.

Beside the non-commutative constraint, geometry appears in a FQH problem in three distinct guises. First, the interaction potential  $\bar{V}_{\mathbf{q}} = V_{\mathbf{q}} |F_m(\mathbf{q})|^2$  is a function of two independent tensors  $g_m$  and  $g_i$  [43], where  $F_m(\mathbf{q}) = \exp(-g_m^{ab} q_a q_b \ell_B^2 / 4)$  is the (lowest) LL form factor and  $V_{\mathbf{q}}$  in general depends on  $\sqrt{g_i^{ab} q_a q_b}$  ( $V_{\mathbf{q}} = 2\pi / \sqrt{g_i^{ab} q_a q_b}$  for the Coulomb interaction). These two tensors are imposed by *extrinsic* experimental conditions, such as the direction of the magnetic field and properties of the underlying solid-state material.  $g_m$  has physical origin in the band mass tensor and can be conveniently parametrized by a  $2 \times 2$  unimodular matrix ( $\det g_m = 1$ )

$$g_m = \begin{pmatrix} \cosh Q + \cos \phi \sinh Q & \sin \phi \sinh Q \\ \sin \phi \sinh Q & \cosh Q - \cos \phi \sinh Q \end{pmatrix}, \quad (2)$$

where  $Q$  and  $\phi$  are real numbers which parametrize a stretch or rotation of the tensor. On the other hand,  $g_i$  is in general different from  $g_m$ . In the case of Coulomb interaction,  $g_i$  originates from the dielectric tensor of the material that hosts the FQH system. Note that both  $g_m$  and  $g_i$  define the shape of some circle:  $g_m$  enters the single-particle wave function thus defining the shape of LL orbitals, while  $g_i$  determines the shape of the interaction equipotentials. They hence effectively measure the distance from the “circle center”, and in this sense we alternatively refer to them as extrinsic metrics [43].

Subject to these two extrinsic metrics, a FQH state develops a third, *intrinsic* geometric degree of freedom. As a many-body property of the system, this intrinsic degree of freedom defines the shape of particle-flux composite droplets in FQH ground states and can also be thought of as a metric  $\hat{g}$  parametrized by the same matrix as in Eq. (2). If the extrinsic metrics are equal ( $g_m = g_i$ ), but not necessarily isotropic ( $\neq \mathbb{1}$ ), the intrinsic metric is equal to them ( $\hat{g} = g_m = g_i$ ) and the physical state is isotropic in a transformed coordinate frame. More gen-

erally, when  $g_m \neq g_i$ ,  $\hat{g}$  is determined from an energetic compromise between  $g_m$  and  $g_i$ , and is in general different from both of them [56, 57]. The intrinsic metric, as an emergent many-body property of the system, will be the main focus of our quench dynamics.

The dynamics of  $\hat{g}$  can in principle be induced by changing the mass tensor,  $g_m$ . While this might be feasible in materials such as ALAs [58], a much more practical way is to tilt the magnetic field [Fig. 1(a)]. Semiclassically, the particles still prefer to make circular orbits around the tilted direction, but because they are confined to a narrow sample, their orbits deform into ellipses in the plane of the FQH system, hence giving rise to an effective mass anisotropy. In fact, assuming parabolic confining potential in the perpendicular direction, tilt can be exactly represented as a  $2 \times 2$  anisotropic mass tensor [56, 59, 60]. Hence, to an excellent approximation we can model the effect of a tilt by an anisotropic mass tensor like in Eq. (2) [59].

Our quench protocol can now be defined as follows: (i) prepare a Laughlin state  $|\psi_0\rangle$  as the ground state of  $H$  with mass tensor  $g_m$ ; (ii) instantaneously change  $g_m \rightarrow g'_m$ ; (iii) evolve in time assuming the system is closed, i.e.,  $|\psi(t)\rangle = \exp(-iH't)|\psi_0\rangle$ , and measure the intrinsic metric as a function of time,  $\hat{g}(t)$ . This protocol is the minimal theoretical model for an experiment where the magnetic field is suddenly tilted. At considerable computational expense, the model can be made more realistic by directly including parallel field (instead of approximating it by mass anisotropy), relaxing the assumption of a closed system, etc. In Appendix C we will consider a particular case of a more realistic, non-instantaneous quench.

The intuition behind geometric quench is the following. In a purely perpendicular field, a FQH state is a low-entangled state of composite objects – particles surrounded by correlation holes of certain size. For example, in the  $\nu = 1/3$  Laughlin state we can view them as electrons in an area corresponding to three magnetic flux quanta [Fig. 1(a)]. These objects have a finite area (fixed by the electron density and total flux through the system), but their shape can vary and is determined by the intrinsic metric  $\hat{g}$  of the FQH state [61], or equivalently by two real parameters,  $Q$  and  $\phi$ , as in Eq. (2). For a weak quench that keeps the system within the Laughlin phase, these droplets are expected to fluctuate and our goal is to determine the equations of motion for  $Q$  and  $\phi$ . This is, however, a highly non-trivial problem because the representation of a state in Fig. 1(a) is merely a cartoon (e.g., the operators projected onto the droplets do not commute with one another).

As emphasized earlier, the key to understanding dynamics are the excited eigenstates in the spectrum of  $H'$ . Such a spectrum for the Laughlin  $\nu = 1/3$  state, obtained by diagonalization of its parent Hamiltonian – the  $V_1$  Haldane pseudopotential [62] – is shown in Fig. 1(b). The low-energy spectrum is dominated by a collective mode known as the Girvin-MacDonald-Platzman (GMP) mode

or “magnetoroton” [55, 63]. This mode is accurately described by the single-mode approximation (SMA), and intuitively represents a density modulation on top of the ground state given by  $\hat{\rho}_{\mathbf{k}}|\psi_0\rangle$ . Such SMA trial wavefunctions were shown to give excellent description of the actual collective excitation for momenta smaller than the magnetoroton minimum [64], both for the exact Laughlin state and the Coulomb ground state. Generalizations of the SMA, based on Jack polynomials, have been shown to be microscopically accurate at *all* values of momenta accessible in finite systems [65].

Since the SMA dominates the low-energy physics of a FQH state, it could be expected that it also plays a crucial role in the quench dynamics. However, this becomes less clear if one notices that our quench protocol preserves the translation symmetry of the initial state, hence all dynamics takes place in  $\mathbf{k} = 0$  sector of the Hilbert space corresponding to the uniform Laughlin state. The  $k \rightarrow 0$  limit of the SMA mode, i.e., the graviton [65], lies inside the 2 quasiparticle-2 quasihole continuum of states [Fig. 1(b)], hence it is far from obvious that quench dynamics can be modelled by this single degree of freedom (although in some cases the  $k \rightarrow 0$  limit of the SMA mode appears to be below the continuum of the energy spectrum [66]).

In the following Section we present results of bimetric theory, which fully incorporates the effects of geometry and the SMA excitation. This theory will show that quenches driven by a  $2 \times 2$  unimodular metric, like in Eq. (2), indeed can be described as the oscillation of a geometric degree of freedom.

### III. WEAK GEOMETRIC QUENCH IN BIMETRIC THEORY

In this Section, we review the bimetric theory developed in Ref. [44], and generalize it to anisotropic quantum Hall states. It will be shown that this generalization provides us with an analytical description of the dynamics of the intrinsic metric  $\hat{g}$  after the geometric quench.

#### A. Lagrangian for the isotropic case

Bimetric theory describes the gapped dynamics of a single spin-2 degree of freedom in a FQH system, interacting with the external electro-magnetic field and ambient geometry. The dynamical degree of freedom is the vielbein  $\hat{e}_i^\alpha$  [67] that “squares” to the dynamic, unimodular metric  $\hat{g}_{ij} = \hat{e}_i^\alpha \hat{e}_j^\beta \delta_{\alpha\beta}$ , or simply  $\hat{g} = \hat{e} \cdot \hat{e}^T$ . Here  $\hat{g}$  corresponds to the intrinsic metric of the FQH state mentioned in the last Section. The inverse metric is given by  $\hat{G}^{ij} = \hat{E}_\alpha^i \hat{E}_\beta^j \delta^{\alpha\beta}$ , where  $\hat{E}_\alpha^i$  is the inverse vielbein [67], satisfying  $\hat{E}_\alpha^i \hat{e}_j^\alpha = \delta_j^i$ . The unimodular condition on  $\hat{g}_{ij}$  takes form  $\sqrt{\hat{g}} = \sqrt{\bar{g}}$ , where  $\sqrt{\bar{g}}$  is the determinant of the *ambient* metric  $g_{ij} = \delta_{AB} e_i^A e_j^B$  and  $e_i^A$  is the ambi-

ent vielbein. Thus, in flat ambient space (that is, when  $g_{ij} = \delta_{ij}$ ),  $\sqrt{\bar{g}} = 1$ .

In the absence of an external electric field, and when the magnetic field is homogeneous, the Lagrangian takes form [44]

$$\mathcal{L} = \frac{\nu\varsigma}{2\pi\ell_B^2} \hat{\omega}_0 - \frac{m}{2} \left[ \frac{1}{2} \hat{g}_{ij} g^{ij} - \gamma \right]^2 = \mathcal{L}_{\text{top}} + \mathcal{L}_{\text{pot}}, \quad (3)$$

where  $\hat{\omega}_0$  is the temporal component of the (dynamic) Levi-Civita spin connection, given by

$$\hat{\omega}_0 = \frac{1}{2} \epsilon_{\alpha\beta} \hat{E}_\beta^i \partial_0 \hat{e}_i^\alpha. \quad (4)$$

The phenomenological coefficient  $m$  sets the energy scale which determines the gap of the spin-2 mode. Quantized coefficient  $\varsigma$  is determined by the “shift”  $\mathcal{S}$  [44] and takes the value  $|\varsigma| = \frac{|\mathcal{S}-1|}{2}$ . The phenomenological parameter  $\gamma$  is used to tune the theory close to the nematic phase transition, where the SMA is exact, in the gapped phase  $\gamma < 1$ . Further details on the bimetric Riemann-Cartan geometry can be found in Refs. [44, 68]. We will utilize it to introduce anisotropy into the problem.

#### B. Anisotropy in bimetric theory

To introduce the quadrupolar anisotropy from a non-trivial mass tensor or other sources, we take the inspiration from Ref. [68], where quadrupolar anisotropy was described in geometric terms. More concretely, we introduce a unimodular matrix  $m_{AB}$ , and construct a rank-2 tensor from it according to

$$g_{ij}^{(m)} = m_{AB} e_i^A e_j^B, \quad (5)$$

where  $e_i^A$  are the vielbeins that describe the ambient geometry. We now generalize Eq. (3) to the anisotropic case. To do so we simply replace  $g_{ij}$  by  $g_{ij}^{(m)}$  in Eq. (3).

To analyze the theory further we make the following simplifying assumptions: (i) the ambient space is assumed to be flat,  $e_i^A = \delta_i^A$ , and (ii) we assume a particular parametrization of  $g_{ij}^{(m)}$ , given by

$$g_{ij}^{(m)} = \begin{pmatrix} e^A & 0 \\ 0 & e^{-A} \end{pmatrix}, \quad (6)$$

where  $A$  is a real parameter that defines the effective anisotropy in the FQH system, which is a compromise between two extrinsic metrics  $g_m$  and  $g_i$  as discussed in the previous Section. Of course, the abrupt change of the mass tensor  $g_m$  in our quench protocol will lead to the change of  $A$  in Eq. (6).

In order to compute the dynamics of  $\hat{g}_{ij}$ , we will parametrize it in terms of  $Q$  and  $\phi$  as in Eq. (2). Both  $Q$  and  $\phi$  are functions of time, but not space, since the problem we will consider is homogeneous (*i.e.*, the quench is

global). The two terms in the Lagrangian take form

$$\mathcal{L}_{\text{top}} = \frac{\bar{\rho}}{2} (1 - \cosh Q) \dot{\phi}, \quad (7)$$

$$\mathcal{L}_{\text{pot}} = -\frac{m}{2} (\gamma + \sinh A \sinh Q \cos \phi - \cosh A \cosh Q)^2. \quad (8)$$

---


$$\dot{\phi} \sinh Q = -2\Omega (\sinh A \cosh Q \cos \phi - \cosh A \sinh Q) (\gamma + \sinh A \sinh Q \cos \phi - \cosh A \cosh Q), \quad (10)$$

and for  $Q(t)$  we find

$$\dot{Q} \sinh Q = -2\Omega \sin \phi \sinh Q \sinh A (\gamma + \sinh A \sinh Q \cos \phi - \cosh A \cosh Q), \quad (11)$$

where we have introduced the energy scale  $\Omega = \frac{m}{\bar{\rho}\varsigma}$ . Eqs. (10) and (11) are the central result of this Section. We will numerically test their validity in the next Section.

### C. Isotropic limit

In the isotropic case we must take  $A \rightarrow 0$ . We find

$$\dot{Q} = 0, \quad \dot{\phi} = 2\Omega (\gamma - \cosh Q). \quad (12)$$

Choosing the solution  $Q = 0$  of the first equation, the second equation reads

$$\dot{\phi} = -2\Omega(1 - \gamma) \equiv -E_\gamma \Rightarrow \phi(t) = \phi(0) - E_\gamma t, \quad (13)$$

from where we interpret  $E_\gamma = 2\Omega(1 - \gamma) = \frac{2m(1 - \gamma)}{\bar{\rho}\varsigma}$  as the gap of the spin-2 part of the GMP mode at  $\mathbf{k} = 0$  [44]. When  $\gamma \rightarrow 1$ , the gap closes and the FQH state undergoes a nematic phase transition [44]. The dynamical metric evaluated on this solution takes form

$$\hat{g}_{ij} = \begin{pmatrix} 1 & 0 \\ 0 & 1 \end{pmatrix}, \quad (14)$$

consequently the dynamics of  $\phi(t)$  is not visible in the fluctuations of the dynamical metric. Formally speaking, this happens because  $Q = 0$ . When  $Q$  is different from 0 the metric will be sensitive to the dynamics of  $\phi$ . This is what happens in the case of weak anisotropy.

### D. Weak geometric quench in bimetric theory

In order to perform the quench described in the previous Section, we have to phrase it in terms of Eqs. (10) and (11). Taking inspiration from Ref. [69], we perform the quench in two steps. First, we need to fix the initial condition  $Q(0), \phi(0)$  for Eqs. (10) and (11), which should be determined by the intrinsic metric of the initial Laughlin state  $|\psi_0\rangle$ . Second, to obtain the quench dynamics, we solve Eqs. (10) and (11) under such initial condition, with the value of  $A$  determined by the effective anisotropy of  $H'$  (or equivalently, by the intrinsic metric of the ground state of  $H'$ ).

The equations of motion are found from

$$\frac{\delta S}{\delta \phi} = 0, \quad \frac{\delta S}{\delta Q} = 0, \quad (9)$$

where  $S = \int d^3x \mathcal{L}$  is the action. The equation for  $\phi(t)$  takes form

---

When anisotropy is weak, both  $A$  and  $Q$  are close to 0. Taylor expansion of Eqs. (10) and (11) in  $A$  and  $Q$  leads to the following system of linear equations

$$\dot{\phi} Q = E_\gamma (A \cos \phi - Q), \quad (15)$$

$$\dot{Q} = E_\gamma A \sin \phi, \quad (16)$$

for which analytical solutions exist under suitable initial conditions. In particular, for  $Q(0) = 0$ , it can be verified by direct substitution that the followings are two exact solutions to Eqs. (15) and (16):

$$Q(t) = 2A \sin\left(\frac{E_\gamma t}{2}\right), \quad \phi(t) = \frac{\pi}{2} - \frac{E_\gamma t}{2}, \quad (17)$$

$$Q(t) = -2A \sin\left(\frac{E_\gamma t}{2}\right), \quad \phi(t) = \frac{3\pi}{2} - \frac{E_\gamma t}{2}, \quad (18)$$

where  $Q$  obeys harmonic motion and  $\phi$  has a simple linear dependence on time. Note that only one of these two solutions is independent because the system is invariant under  $Q \rightarrow -Q$  and  $\phi \rightarrow \phi + \pi$ .

As long as the quench is weak, the linearized Eqs. (15) and (16) provide a remarkably accurate approximation to the full non-linear dynamics. Fig. 2 shows the comparison of the numerical solutions of non-linear Eqs. (10) and (11) satisfying  $Q(0) = 0$  against their linearized counterparts Eqs. (17) and (18), where we focus on the  $Q \geq 0$  part and consider  $\phi \bmod 2\pi$ . Red solid lines in Fig. 2 result from a combination of Eqs. (17) and (18), which gives us  $Q$  and  $\phi$  as periodic functions with frequency  $E_\gamma$ . Since Eqs. (15) and (16) are an accurate approximation of Eqs. (10) and (11) in the weak quench regime, we will compare the solution of Eqs. (15) and (16) against the numerical results obtained in the following Sections. We have checked that fitting the numerical results against the solution of Eqs. (15) and (16) gives very similar  $A$  and  $E_\gamma$  to the fits against the solution of non-linear Eqs. (10) and (11) in the weak quench regime.

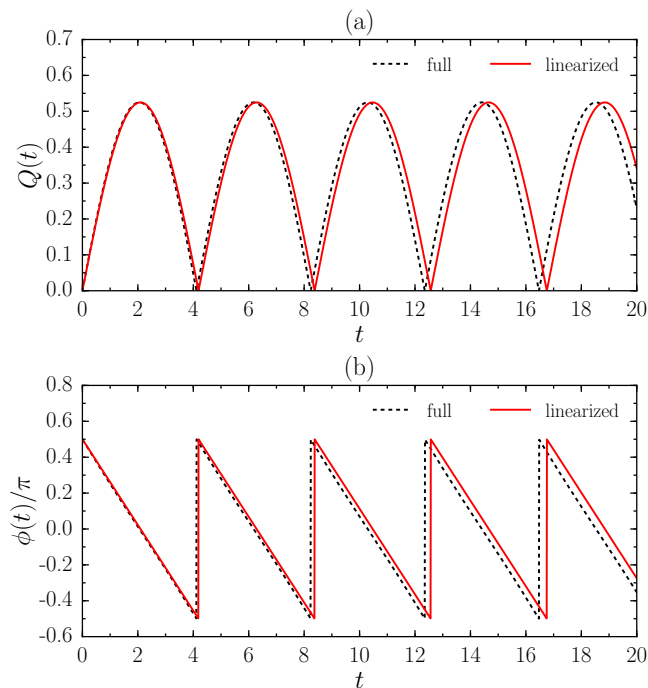


FIG. 2. Predictions of bimetric theory for (a)  $Q$  and (b)  $\phi$  under the initial condition  $Q(0) = 0$ . Black dashed lines indicate the numerical solution of the full equations, Eqs. (10) and (11). Red solid lines indicate the analytical solution Eqs. (17) and (18) of the linearized system, Eqs. (15) and (16). Here we focus on the  $Q \geq 0$  solution. The parameters are fixed at  $\Omega = 1.5/4$ ,  $\gamma = -1$ ,  $A = \ln 1.3$ .

#### IV. NUMERICAL METHOD

Our numerical calculations are carried out using the Hamiltonian in Eq. (1) for  $N$  particles and  $N_\Phi$  flux quanta on a square torus [Fig. 3(a)]. Magnetic translation operators [70] are used to reduce the complexity of the Hamiltonian and to classify the many-body eigenstates. We focus on the Laughlin states of bosons and fermions, corresponding to filling factors  $\nu = 1/2$  and  $\nu = 1/3$ , respectively.

We consider two types of interaction potentials. In the first case, we assume model (short-range) interaction for which the Laughlin state is the unique (and the densest) zero-energy state [71]. This interaction is a simple contact repulsion for bosons,  $V_{\mathbf{q}} = 1$ , and for fermions it is  $V_{\mathbf{q}} = L_1(g_m^{ab} q_a q_b)$ , where  $L_1$  is the first Laguerre polynomial. As customary in the literature [43], in the model interaction we have assumed that the interaction metric  $g_i$  coincides with the Landau orbit metric  $g_m$ . In the second case, we consider Coulomb interaction, for which  $g_i$  is kept isotropic, i.e.,  $V_{\mathbf{q}} = 2\pi/\sqrt{q_x^2 + q_y^2}$ , but the mass tensor  $g_m$  is allowed to be non-isotropic.

For both types of interaction, the quench is implemented by switching  $g_m$  to  $g'_m$  at time  $t = 0$ , where both  $g_m$  and  $g'_m$ , for simplicity, are taken to be diag-

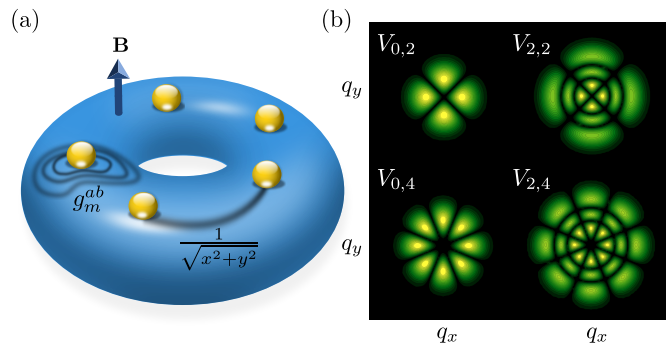


FIG. 3. (a) A FQH system on the surface of a torus threaded by perpendicular magnetic field. The mass tensor  $g_m$  determines the metric of the Landau level orbitals and is used to drive a quench, while the Coulomb potential is assumed to be isotropic. (b) Contours in momentum space of the leading order anisotropic pseudopotentials for bosons [52] with quadrupolar ( $V_{0,2}$ ,  $V_{2,2}$ ) and octupolar ( $V_{0,4}$ ,  $V_{2,4}$ ) structure.

onal, like in Eq. (6). For small system sizes, the subsequent time evolution is performed by obtaining all energy eigenvalues  $\epsilon_n$  and corresponding eigenvectors  $|n\rangle$  of the quench Hamiltonian  $H'$ , and then evaluating  $|\psi(t)\rangle = \sum_n \exp(-i\epsilon_n t) \langle n|\psi_0\rangle |n\rangle$ . By restricting the sum to a subset of eigenstates, one can conveniently project the dynamics onto a desired energy shell. At larger system sizes, we use time-dependent Lanczos methods to iteratively compute  $|\psi(t)\rangle$ .

We use the same parametrization for the intrinsic metric  $\hat{g}$  as in Eq. (2). Due to its invariance under  $Q \rightarrow -Q$  and  $\phi \rightarrow \phi + \pi$ , we focus on  $Q \geq 0$ . For a given state  $|\psi(t)\rangle$ ,  $\hat{g}$  is determined by brute force search over a large set of (precomputed) trial states  $|\psi_{\text{trial}}\rangle$ , i.e., model Laughlin states parametrized by  $Q \in [0, Q_{\text{max}}]$  and  $\phi \in [-\pi, \pi]$ , such that the overlap  $|\langle \psi_{\text{trial}}|\psi(t)\rangle|$  is maximized. For weak quenches, we found it sufficient to restrict to  $Q_{\text{max}} = 1$  and  $\phi \in [-\pi/2, \pi/2]$ , as can be inferred from Fig. 2. The confidence in the result is quantified by the maximum overlap achieved: if this overlap is not close to 1, none of the trial states appropriately describes the system and the intrinsic metric should be determined via some other means, for example via minimization of total energy or momentum polarization [68].

Finally, in order to identify states corresponding to the spin-2 excitation, we use the recently developed formalism of anisotropic pseudopotentials [52]. In Ref. [52] it was shown that any two-particle interaction, including cases where metrics  $g_m$  and  $g_i$  are different, can be expanded into an orthonormal basis of generalized pseudopotentials. These operators maintain translation invariance, but break rotation symmetry to a discrete subgroup. Up to normalization prefactors, the generalized pseudopotentials are given by [52]

$$V_{m,n}(g_p; q_x, q_y) = L_m^n(g_p^{ab} q_a q_b) \mathbf{q}^n + \text{c.c.}, \quad (19)$$

where  $m, n$  are even integers (for bosons). When  $n = 0$ ,

these reduce to the usual (isotropic) Haldane pseudopotentials [71].  $V_{m,n}$  explicitly depends on the metric  $g_p$  through the argument of the Laguerre polynomial, as well as the vector  $\mathbf{q}$ . For simplicity, we fix  $g_p = \mathbb{1}$  and  $\mathbf{q} = \frac{1}{\sqrt{2}}(q_x + iq_y)$  in our following numerics.

Contours of leading-order  $V_{m,n}$  for bosons are depicted in Fig. 3(b). In particular, we can observe that the dominant pseudopotential  $V_{0,2}$  has a clear quadrupolar structure in momentum space, indicating that  $\hat{V}_{0,2}$  carries angular momentum  $L_z = 2$ . Based on this, we can use  $\hat{V}_{0,2}$  as a spectroscopic probe of states which are part of spin-2 excitation. To that end, we introduce the following “spectral function”:

$$I_{m,n}(\omega) = \sum_j \delta(\omega - \epsilon_j) |\langle j | \hat{V}_{m,n} | 0 \rangle|^2. \quad (20)$$

This is a generalization of the spectral function that describes an acoustic wave absorption experiment [72]. The peaks of  $I_{m,n}$  are expected to yield the frequencies of different spin modes in the quench dynamics. In Sec. V we investigate in detail  $I_{0,2}$  and show that it indeed yields the frequency of the graviton mode.

## V. RESULTS

Now we present our numerical results for finite systems and compare them with the predictions of bimetric theory. We focus on weak quenches, where the mass tensor is instantaneously changed from  $g_m = \text{diag}(e^{A_0}, e^{-A_0})$  to  $g'_m = \text{diag}(e^{A_1}, e^{-A_1})$  with  $A_0$  and  $A_1$  close to 0. By scanning the overlap between the post-quench state and a set of anisotropic model Laughlin states, we find that the maximal overlap is always high, which means that the post-quench state stays in the Laughlin phase. The intrinsic metric  $\hat{g}$  of the post-quench state is determined by the maximum of this overlap. In the following, we focus on the dynamics of  $\hat{g}$  for  $\nu = 1/2$  bosons in detail, while similar results for  $\nu = 1/3$  fermions are given in Appendix D. In all numerical data below, time is given in units of inverse energy [ $e^2/(\epsilon\ell_B)$  in the case of Coulomb interaction], with  $\hbar = 1$ .

### A. Isotropic-to-anisotropic quench

We start from the simple case of  $A_0 = 0, A_1 > 0$ , where the initial state is an isotropic Laughlin state. With the initial condition  $Q(0) = 0$ , the bimetric theory predicts that the post-quench dynamics of  $\hat{g}$  (parameterized by  $Q$  and  $\phi$ ) is governed by Eqs. (17) and (18). As representative examples, we choose  $A_1 = \ln 1.3$  and  $A_1 = \ln 2.0$  for quenches driven by contact and Coulomb interactions, respectively. Exact dynamics of  $\hat{g}$  up to moderate times is shown in Figs. 4 and 5 for these two types of interactions. Indeed,  $Q$  and  $\phi$  behave in accordance with the predictions of bimetric theory for both interactions. In

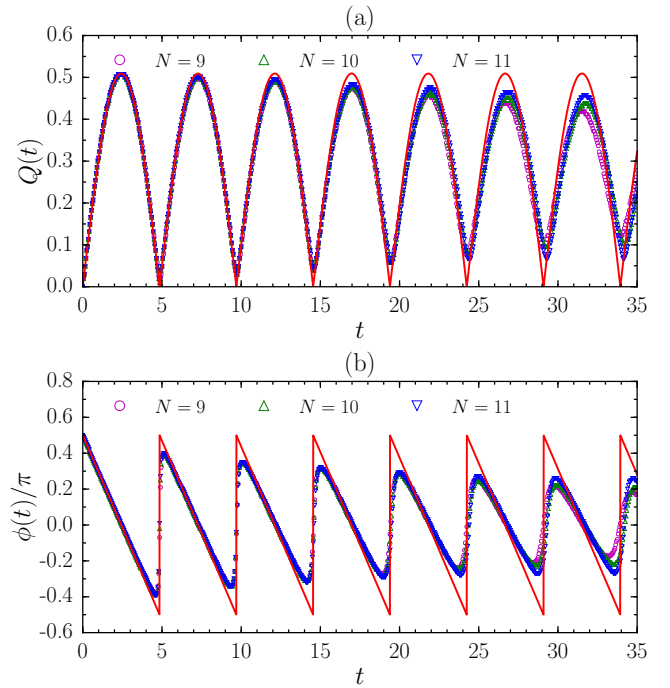


FIG. 4. Exact dynamics of (a)  $Q$  and (b)  $\phi$  for  $N = 9 - 11$  bosons at  $\nu = 1/2$  with the contact interaction. The weak geometric quench is driven by choosing  $A_0 = 0$  and  $A_1 = \ln 1.3$ . The red solid curve is the  $Q \geq 0$  part of Eqs. (17) and (18), with  $A \approx 0.255$  and  $E_\gamma \approx 1.296$ . These two parameters are obtained by fitting the first oscillation of  $Q$  of  $N = 11$  against the solution.

particular, we can fit the the numerical data at small  $t$  (corresponding to the first one or two oscillations) against Eqs. (17) and (18), with remarkable agreement (red solid lines in Figs. 4 and 5). The fits lie on top of numerical data and convincingly indicate that the short-time dynamics of  $\hat{g}$  fully agrees with bimetric theory. Note that even though we consider a regime of weak quench here, the induced change in the microscopic structure of the FQH state is by no means small: for the above choices of  $A_1$  in Figs. 4 and 5, we find the maximum anisotropy  $e^Q$  of the post-quench state to be larger than the initial (isotropic) state by a factor 1.5 – 2.5.

The fits of numerical data into Eqs. (17) and (18) allow us to extract the values of  $A$  and  $E_\gamma$  in bimetric theory.  $A$  quantifies the intrinsic anisotropy in the ground state of  $H'$ , which is a compromise between  $g'_m$  and  $g'_i$ . Since we do the same modification for  $g_m$  and  $g_i$  in the quench driven by the contact interaction, we expect  $A = A_1$  in this case. Indeed, we get  $A \approx 0.255$  from the fit in Fig. 4, which is very close to  $A_1 = \ln 1.3 \approx 0.262$ . However, in the quench driven by the Coulomb interaction, we keep isotropic  $g_i$  and only change  $g_m$ , so the intrinsic anisotropy in the ground state of  $H'$  is expected to be weaker than  $g'_m$ . The fit in Fig. 5 gives  $A \approx 0.454$ , which is indeed between 0 and  $A_1 = \ln 2.0 \approx 0.693$ .

The second parameter,  $E_\gamma$ , is interpreted as the gravi-

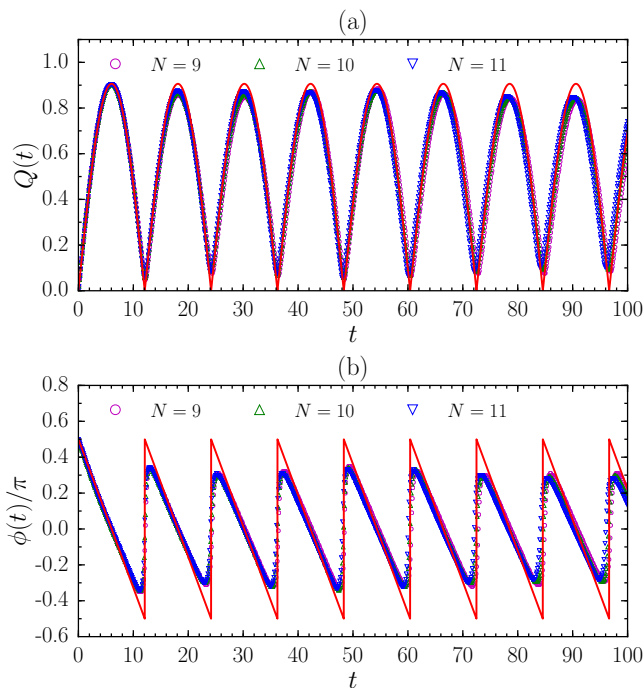


FIG. 5. Exact dynamics of (a)  $Q$  and (b)  $\phi$  for  $N = 9 - 11$  bosons at  $\nu = 1/2$  with the Coulomb interaction. The weak geometric quench is driven by choosing  $A_0 = 0$  and  $A_1 = \ln 2.0$ . The red solid curve is the  $Q \geq 0$  part of Eqs. (17) and (18), with  $A \approx 0.453$  and  $E_\gamma \approx 0.520$ . These two parameters are obtained by fitting the first oscillation of  $Q$  of  $N = 11$  against the solution.

ton gap in bimetric theory. By extracting this parameter from the fitting of quench data for various initial parameters, we find that the obtained  $E_\gamma$  is indeed insensitive to the precise values of  $A_0$  and  $A_1$ , as long as we are in the weak quench regime. For the specific quenches in Figs. 4 and 5, we obtain  $E_\gamma \approx 1.296$  and  $0.520$ , respectively. We can thus estimate the graviton gap as  $\approx 1.3$  for the contact interaction and  $0.52$  for the Coulomb interaction.

Since the graviton mode carries spin 2, we can alternatively use the  $I_{0,2}(\omega)$  spectral function defined in Eq. (20) as its independent probe. We expect peaks of  $I_{0,2}(\omega)$  at energies corresponding to the spin-2 excitations that comprise the graviton mode. In Fig. 6, we show  $I_{0,2}(\omega)$  (normalized by  $\int I_{0,2}(\omega)d\omega$ ) for contact and Coulomb interactions in isotropic systems (similar data are obtained for weakly anisotropic systems). In the case of contact interaction, we indeed observe sharply pronounced peaks of  $I_{0,2}(\omega)$  around  $\omega = 1.3$  for various system sizes [Fig. 6(a)], which means that spin-2 eigenstates concentrate in this narrow energy window, corresponding to the graviton gap  $\omega \approx 1.3$ . For Coulomb interacting systems, a pronounced peak in  $I_{0,2}(\omega)$  also exists, but at a lower energy  $\omega = 0.55$  [Fig. 6(b)]. These estimations of the graviton gap using the  $I_{0,2}(\omega)$  spectral function very accurately match those obtained from the dynamical prediction of bimetric theory. As a third way of estimating

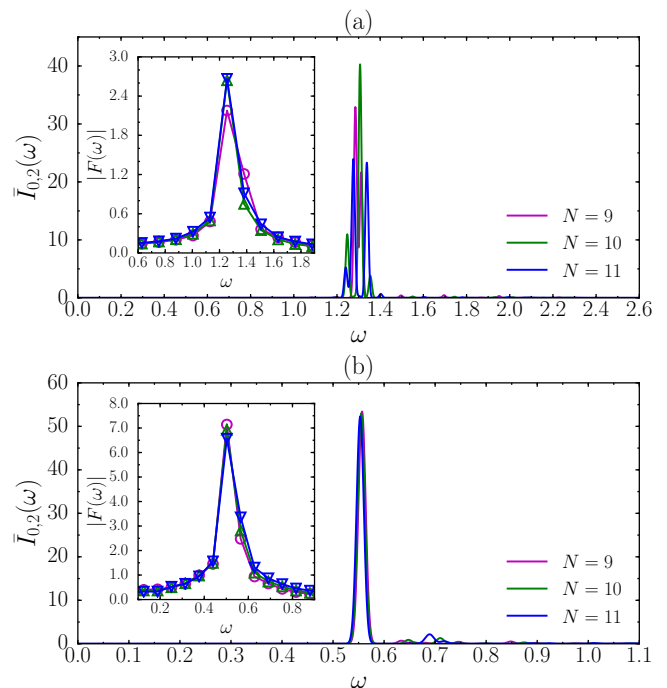


FIG. 6. Normalized spectral function  $\bar{I}_{0,2}(\omega) = I_{0,2}(\omega) / \int I_{0,2}(\omega)d\omega$  for isotropic systems of  $N = 9 - 11$  bosons at  $\nu = 1/2$  with (a) contact and (b) Coulomb interactions. The insets show the discrete Fourier transform  $|F(\omega)|$  of  $Q$  in Figs. 4 and 5. Markers in insets and curves in main figures with the same color refer to the same system size.

the graviton gap, we can use the discrete Fourier transform of  $Q$  (see insets of Fig. 6). This Fourier transform also shows a sharp peak around the same energy as that in  $I_{0,2}(\omega)$ , which further confirms that the dynamics of the intrinsic metric is indeed caused by the graviton oscillation.

In summary, for weak isotropic-anisotropic quenches we find excellent agreement between exact dynamics and predictions of bimetric theory based on the harmonic motion of a single spin-2 degree of freedom. Minor deviations from bimetric theory can be observed in Figs. 4 and 5 at longer times. These deviations generally have two manifestations: as a decay in amplitude while maintaining the overall oscillation structure, or as a total departure from the oscillation. The former is mainly the case for isotropic-to-anisotropic quenches considered in Figs. 4 and 5, while the latter can be observed in a more general case of anisotropic-to-anisotropic quench considered in Appendix A as well as in some fermionic data in Appendix D. There are two possible reasons for these discrepancies. First, finite-size effects might be at play. In particular, in finite systems a “fragmentation” of the spin-2 graviton mode into several states with large matrix element  $|\langle n | \hat{V}_{0,2} | 0 \rangle|^2$  (as seen in Fig. 6) induces several close frequencies in the dynamics. With the available data for system sizes up  $N = 12$ , there is no clear indication that this effect disappears in the thermodynamic

limit, even though a “sharp” spin-2 mode is theoretically anticipated in large systems. Moreover, the finite-size effects in the dynamics at longer times would also come from an effective Lieb-Robinson [73] “light cone” exceeding the finite-size of the system. The second reason for the discrepancy is a possible contribution of higher-spin modes to the dynamics. Those are not included in bimetric theory, but our generalized quenches in Sec. VI strongly suggest that these modes do exist and could contribute to the quench, especially at longer times.

### B. States contributing to dynamics

Excellent agreement between the exact dynamics of  $\hat{g}$  and the oscillation of the spin-2 graviton mode strongly implies that the exact dynamics is dominated by spin-2 eigenstates of  $H'$ . We now scrutinize this conjecture by quantifying how well the full dynamics can be reproduced by an explicit projection to a subset of eigenstates centered around the the energy of the spin-2 mode.

The projected subspace is defined by the eigenstates  $|n\rangle$  of  $H'$  with dominant matrix elements  $|\langle n|\hat{V}_{0,2}|0\rangle|^2$ . The weight of this projection is measured by  $f = \left(\sum_{n=0}^{M-1} |\langle n|\hat{V}_{0,2}|0\rangle|^2\right) / \left(\sum_{n=0}^{D-1} |\langle n|\hat{V}_{0,2}|0\rangle|^2\right)$ , where  $|n\rangle$  have been sorted in descending order according to  $|\langle n|\hat{V}_{0,2}|0\rangle|^2$ . Here  $M$  is the number of kept states and  $D$  is the total number of eigenstates that we can obtain from exact diagonalization of  $H'$ :  $D$  is equal to the Hilbert space dimension in the  $\mathbf{k} = 0$  sector for  $N \leq 9$ , while for practical reasons we kept  $D = 200$  for larger systems ( $N = 10 - 12$ ). Remarkably, the number of states we need to saturate the total weight  $f$  is significantly smaller than the Hilbert space dimension. Fixing  $f = 99\%$ , the finite-size scaling of the required  $M$  clearly indicates that only an exponentially small fraction of the whole Hilbert space carries spin-2, as shown in Fig. 7.

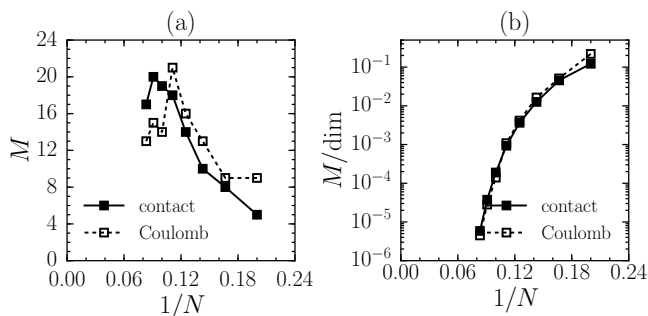


FIG. 7. Finite-size scaling of the number of spin-2 states in the  $\mathbf{k} = 0$  Hilbert space for  $N = 5 - 12$  bosons at  $\nu = 1/2$ .  $M$  represents the number of states which contain  $f = 99\%$  of the total  $|\langle n|\hat{V}_{0,2}|0\rangle|^2$ . We consider both contact and Coulomb quench Hamiltonians, with  $A_1 = \ln 1.3$  and  $A_1 = \ln 2.0$ , respectively. The plots show (a)  $M$  and (b)  $M/\text{dim}$ , where  $\text{dim}$  is the  $\mathbf{k} = 0$  Hilbert space dimension.

While the exponentially decaying ratio of  $M$  to the Hilbert space dimension might not be entirely surprising (since it still does not preclude  $M$  being exponentially large in the system size), it can also be shown that, in absolute terms, only a very small number of states  $M$  yields a very accurate approximation to the exact dynamics. In Appendix B, we perform the above projection, based on the  $|\langle n|\hat{V}_{0,2}|0\rangle|^2$  matrix elements, for the dynamics of  $N = 11$  bosons driven by the isotropic-to-anisotropic quench (Fig. 10). Remarkably, the main features of the exact dynamics are already accurately reproduced for  $M$  less than 10, even if there are as many as 533160 eigenstates in the entire  $\mathbf{k} = 0$  Hilbert space. Such an excellent approximation of the exact dynamics by an exponentially small fraction of states in the Hilbert space is another evidence for the picture of graviton oscillation that underpins bimetric theory.

## VI. HIGHER-SPIN MODES

Tuning the anisotropy of the mass tensor is an experimentally relevant mechanism for changing the metric in the interaction. However, this also leads to the modification of the entire set of coefficients  $c_{m,n}$  of the generalized Haldane pseudopotentials  $\hat{V}_{m,n}$  [Eq. (19)] which characterize the interaction:  $\hat{V}_{\mathbf{q}} = \sum_{m,n} c_{m,n} V_{m,n}(\mathbf{q})$ . For theoretical purposes, modifying individual coefficients  $c_{m,n}$ , one at a time, is a much more controlled way to drive a quench. This new quench protocol brings more freedom to probe the dynamics. As we will show below, reformulating the quench protocol in this way not only includes the former scenario of changing the mass tensor, but also exposes new types of dynamics which are invisible to bimetric theory.

We first assume that all  $c_{m,n}$ 's are initially zero except  $c_{0,0} = 1$ , then a nonzero  $c_{0,2} = 0.1$  is introduced at  $t = 0^+$ . This corresponds to a modification of the interaction  $\hat{V}_0 \rightarrow \hat{V}_0 + 0.1\hat{V}_{0,2}$ . Since  $\hat{V}_{0,2}$  carries angular momentum  $L_z = 2$ , we expect that its presence will drive a quench dominated by spin-2 excitations. Indeed, we find that the consequent exact dynamics of  $\hat{g}$  again falls into the description of spin-2 graviton oscillation [Fig. 8(a)] and is very similar to that driven by changing the mass tensor (Fig. 4).

Next we consider a quench driven by adding a small amount of  $\hat{V}_{0,4}$  component ( $c_{0,4} = 0.1$ ) such that the interaction changes according to  $\hat{V}_0 \rightarrow \hat{V}_0 + 0.1\hat{V}_{0,4}$  at  $t = 0^+$ . This type of quench could be realized in systems whose Fermi contours are not simple ellipses, e.g., where the band dispersion has the form  $\epsilon(\mathbf{k}) = k^N \cos(N\theta)$  [74, 75]. As shown in Ref. [75], when  $N = 4$ , the dominant pseudopotential is  $V_{0,4}$  (with a caveat that the maximum magnitude of anisotropic pseudopotentials that can be achieved by varying the mass tensor is smaller for  $N = 4$  than for the familiar elliptic case, i.e.,  $N = 2$ ).

For the quench driven by  $\hat{V}_{0,4}$ , the numerical result is completely different from bimetric theory. Instead of os-

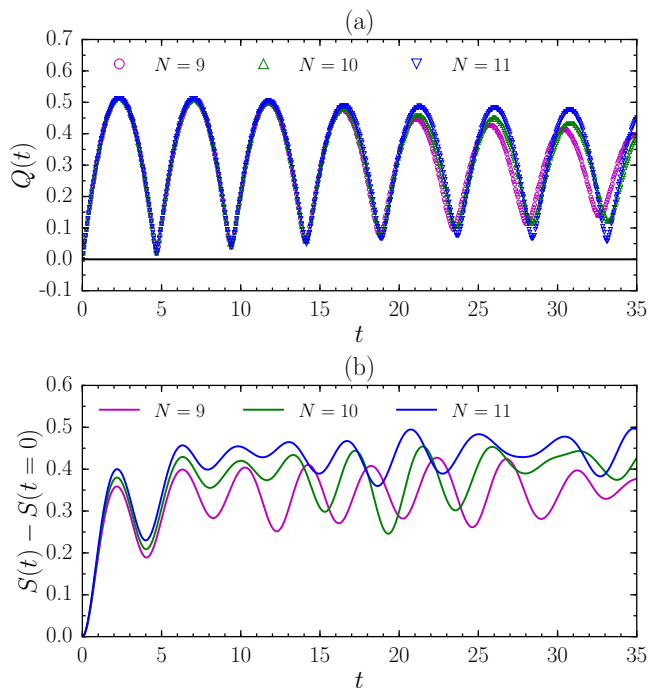


FIG. 8. (a) Exact dynamics of  $Q$  for the quench with  $\hat{V}_0 \rightarrow \hat{V}_0 + 0.1\hat{V}_{0,2}$  (color symbol) and  $\hat{V}_0 \rightarrow \hat{V}_0 + 0.1\hat{V}_{0,4}$  (black solid line). We notice a complete absence of dynamics of  $\hat{g}$  in the case of the perturbation by  $\hat{V}_{0,4}$ . (b) Growth of entanglement entropy after a quench with  $\hat{V}_0 \rightarrow \hat{V}_0 + 0.1\hat{V}_{0,4}$ . Both plots show data for  $N = 9 - 11$  bosons at  $\nu = 1/2$ .

cillations, we find  $Q(t) = 0$  during the entire measured time interval [see the black solid line in Fig. 8(a)]. This means that, surprisingly, there is no dynamics of  $\hat{g}$  in this case. Of course, the system does respond to the perturbation by  $\hat{V}_{0,4}$  in various other ways to which  $\hat{g}$  is not sensitive. For example, the time dependence of entanglement entropy shows that the post-quench state  $|\psi(t)\rangle$  clearly evolves with time [Fig. 8(b)]. We define entropy by dividing all LLL orbitals into two equal halves  $A$  and  $B$ , and calculating  $S(t) = -\text{Tr}(\rho_A \ln \rho_A)$ , where the reduced density matrix is  $\rho_A = \text{Tr}_B(|\psi(t)\rangle\langle\psi(t)|)$ . As a non-local quantity, entanglement entropy is a convenient measure of all types of dynamical processes that might be taking place in the system. Clear oscillations in  $S(t)$  are a convincing signature of the non-trivial quench dynamics.

The failure of bimetric theory to capture the quench dynamics driven by  $\hat{V}_{0,4}$  strongly suggests that the  $\hat{V}_{0,4}$  quench is dominated by higher-spin excitations rather than spin-2 ones. Indeed, unlike the quadrupolar  $\hat{V}_{0,2}$ ,  $\hat{V}_{0,4}$  has octupolar structure in momentum space [Fig. 3(b)], which implies that it carries higher angular momentum and couples to higher-spin excitations (e.g., spin-4). Also, this result provides an unambiguous example in which the  $2 \times 2$  unimodular metric in Eq. (2) is inadequate to capture the anisotropy in the Laughlin

state, motivating a generalization of the geometrical description of the Laughlin states and the associated field theory.

## VII. CONCLUSIONS AND OUTLOOK

In the present manuscript we have laid out the theoretical foundation for studying the non-equilibrium dynamics of FQH states. Utilizing the recently developed anisotropic pseudopotentials and bimetric theory, we have proposed and numerically simulated the geometric quench protocol which excites certain neutral collective degrees of the FQH liquid. We have analyzed the dynamics for the Hamiltonians for which the Laughlin states of bosons at  $\nu = 1/2$  and of fermions at  $\nu = 1/3$  are exact ground states, as well as for the Coulomb interaction. In all these cases, we have found that the short-time dynamics after the geometric quench is very accurately described by the bimetric theory – a geometric theory of collective, spin-2 excitation supported by the FQH liquid.

We have demonstrated that the quench protocol admits an interesting generalization that allows one to excite higher-spin collective degrees of freedom, whose dynamics cannot be described by the currently available theoretical concepts. We believe that the present work will motivate a more detailed study of the geometric degrees of freedom in various strongly correlated systems. Below we outline several other exciting directions that open up for future investigations.

The immediate question which arises is the experimental applicability of our results. Even though the quench protocol can in principle be directly implemented with the available technology, the main challenges are the usual difficulty in observing coherent dynamics in solid-state systems (in our case, due to the smallness of the magnetic length), and the experimental measurement of the intrinsic metric in gapped FQH states. Regarding the latter point, several state-of-the-art experiments have succeeded in measuring the anisotropy of the composite fermion Fermi surface induced by tilting the magnetic field [29, 76]. Similar measurements were also performed for hole systems [77]. However, such experiments still need to be generalized to gapped FQH states (we note that acoustic wave absorption has been theoretically proposed as an alternative spectroscopic probe of the graviton [72]). Thus, at this stage, the geometric FQH quench remains of primarily theoretical interest.

A number of new theoretical questions can be formulated using the quench protocol. For example, new dynamical phenomena will likely arise in Abelian FQH states with more complicated internal structure, such as bi-layer states and Jain states. These states host multiple collective modes which would all contribute to the dynamics. Multi-layer systems feature rich phase diagrams that can be explored by tuning the interaction strength between the layers [78, 79]. It would be interesting to

map out the dynamical counterparts of such equilibrium phase diagrams by studying the geometric quench in different interaction regimes.

Even in the simplest models of Laughlin states, our study has focused on the linear weak quench regime. The non-linear regime should become relevant for strong quenches as well as for the dynamics close to the nematic phase transition. The present quench protocol could be used as a complementary tool for probing the nematic transition, which has recently been studied in Ref. [80]. The current difficulty in accessing the non-linear regime in the numerics is due to the inefficient procedure for determining the intrinsic metric. The formulation of a more robust measure of the intrinsic metric, which does not rely on a specific trial state, is an important open problem.

We have argued that when a “higher-spin” pseudopotential drives the quench, the spin-2 mode can remain unexcited, while the system clearly undergoes non-trivial dynamics. It is likely that a richer set of trial states is needed to fully describe such dynamics. This set of states should be parametrized by higher-spin cousins of the intrinsic metric  $\hat{g}$ . Similar conclusions were reached in Ref. [44] (see also Ref. [81]) where the bimetric theory was argued to be a low-energy approximation to a more complicated higher-spin theory, and in Ref. [51] where the linearized bimetric for the Jain series at  $\nu = n/(2n + 1)$  was derived from the Dirac composite Fermi liquid (CFL) theory at large  $n$ . In the latter approach the higher-spin modes naturally emerge as collective distortions of the composite Fermi surface. In fact, when the CFL state forms, all of the higher-spin degrees of freedom become gapless, and are equally important for the dynamics. In these systems, the geometric quench described in the present manuscript, as well as its “higher-spin” cousins, will provide an interesting probe of the collective dynamics of the composite fermion Fermi surface.

The geometric quench also presents an exciting possibility of probing the non-Abelian fractional quantum Hall states, such as the Moore-Read state [9] – a candidate for the observed  $\nu = 5/2$  plateau [82]. Numerical works [83, 84] have shown that the Moore-Read state hosts a neutral fermionic mode, in addition to the SMA (bosonic) mode. The neutral fermion mode is expected to have angular momentum  $3/2$  and is not present in the bimetric theory. It would be very interesting to design the effective theory and numerical probes of this mode at long wavelengths.

Finally, fractional Chern insulators (FCIs) exhibit much of the same phenomenology as the FQH states (see the recent reviews Refs. [85–87] and references therein). For example, the FCIs also feature the GMP algebra [88, 89], the intrinsic metric [90], and they naturally correspond to anisotropic FQH states [52, 91]. In particular, the FCI states in higher Chern number bands [92–94] do not have usual continuum FQH states as counterparts [95], therefore it would be interesting to study their SMA modes and the dynamics following a geometric quench.

## VIII. ACKNOWLEDGEMENTS

We thank V. Caudrelier for illuminating discussions about the system of differential equations. This work was supported in part by the Department of Energy, Office of Basic Energy Sciences through Grant No. DE – SC0002140. Z.L. was supported by Alexander von Humboldt Research Fellowship for Postdoctoral Researchers. A.G. was supported by the Leo Kadanoff fellowship, the NSF grant DMR-1206648, and by the University of Chicago Materials Research Science and Engineering Center, which is funded by the National Science Foundation under award No. DMR-1420709. Z.P. acknowledges support by EPSRC grant EP/P009409/1. Statement of compliance with EPSRC policy framework on research data: This publication is theoretical work that does not require supporting research data.

### Appendix A: Anisotropic-to-anisotropic quench

As an immediate generalization of the isotropic-to-anisotropic quench studied in Sec. V A, we now discuss the more general case of a quench with  $A_1 > A_0 > 0$ , for which the initial state is already anisotropic. In this case, simple analytical solutions does not exist under the general initial conditions  $Q(0) > 0, \phi(0) = 0$  even for the linearized systems Eqs. (15) and (16). However, by numerically solving the coupled differential equations, we find that bimetric theory still accurately describes the short-time dynamics of  $Q$  and  $\phi$ , and also captures the oscillatory dynamics very well up to moderate times.

In Fig. 9, we choose  $A_0 = \ln 1.3$  and  $A_1 = \ln 1.7$ , and show the exact dynamics for the quench driven by the contact interaction. Since the initial state is a Laughlin model state with  $\hat{g}(0) = g_m$ , the bimetric theory predicts the post-quench dynamics of  $\hat{g}$  is governed by the solution of Eqs. (15) and (16) with initial condition  $Q(0) = A_0, \phi(0) = 0$ . Indeed, the numerical data in the first two periods again lie on top of such solution with fitting parameters  $A \approx 0.523$  and  $E_\gamma \approx 1.283$ . The value of  $A$  is close to  $A_1 = \ln 1.7 \approx 0.531$  as expected, and  $E_\gamma \approx 1.283$  is consistent with the graviton gap estimated from both the  $I_{0,2}(\omega)$  spectral function and the previous fit in Fig. 4.

As discussed in Sec. V A, apart from generally good agreement, we can also observe some discrepancy between the exact dynamics and the equations of bimetric theory in Fig. 9. This discrepancy is likely caused by the mentioned finite-size effect (the splitting of the spin-2 mode into several states and the Lieb-Robinson light cone) and the possible contribution of higher-spin modes. Compared to isotropic-to-anisotropic quench, stronger finite-size effects in the present case are not surprising because anisotropy effectively reduces the length of the system along one of the spatial directions.

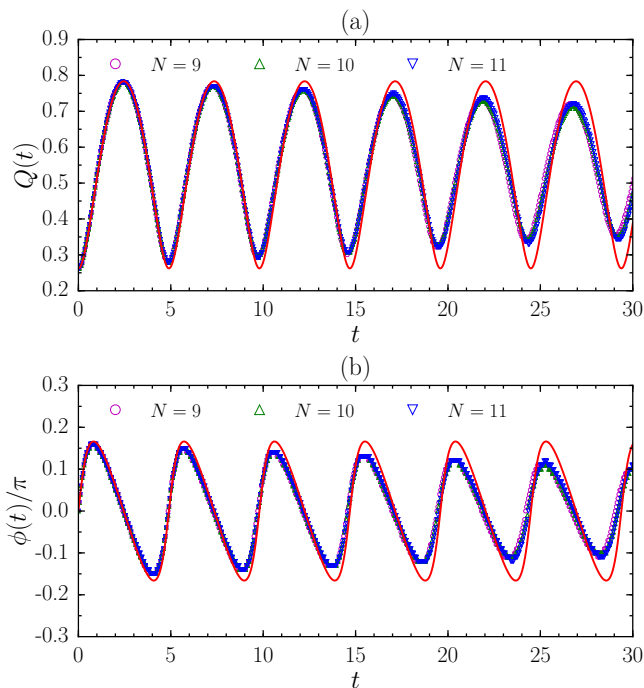


FIG. 9. Exact dynamics of (a)  $Q$  and (b)  $\phi$  for  $N = 9 - 11$  bosons at  $\nu = 1/2$  with the contact interaction. The weak geometric quench is driven by choosing  $A_0 = \ln 1.3$  and  $A_1 = \ln 1.7$ . The red solid curve is the solution of linearized equations Eqs. (15) and (16) under the initial condition  $Q(0) = A_0, \phi(0) = 0$ , with  $A \approx 0.523$  and  $E_\gamma \approx 1.283$ . These two parameters are obtained by fitting the first oscillation of  $Q$  of  $N = 11$  against the solution.

### Appendix B: Projected dynamics

In the main text, we have shown that the number of spin-2 eigenstates of  $H'$  is exponentially smaller than the full Hilbert space dimension. The number of spin-2 eigenstates was determined by the matrix element of  $\hat{V}_{0,2}$  generalized pseudopotential. Here we investigate how accurately the quench dynamics can be reproduced by projecting to this set of states.

We perform the projection explicitly, i.e., we calculate the post-quench state as  $|\tilde{\psi}(t)\rangle = \frac{1}{\mathcal{N}} \sum_{n \in \mathcal{S}} \exp(-i\epsilon_n t) \langle n | \psi_0 \rangle |n\rangle$ , where  $\mathcal{S}$  contains the first  $M$  eigenstates with the largest  $|\langle n | \hat{V}_{0,2} | 0 \rangle|^2$  matrix elements and  $\mathcal{N}$  is the normalization factor. The dynamics of the intrinsic metric of  $|\tilde{\psi}(t)\rangle$  after an isotropic-anisotropic quench is shown in Fig. 10 for  $N = 11$  bosons, together with the exact dynamics without projection. As expected, the projected dynamics approaches the exact dynamics with increasing  $M$ . However, for both contact and Coulomb interactions, the main feature in exact dynamics has been accurately reproduced by  $M$  less than 10, even if the whole Hilbert space in this case is more than four orders of magnitude larger. Such an excellent approximation of the exact

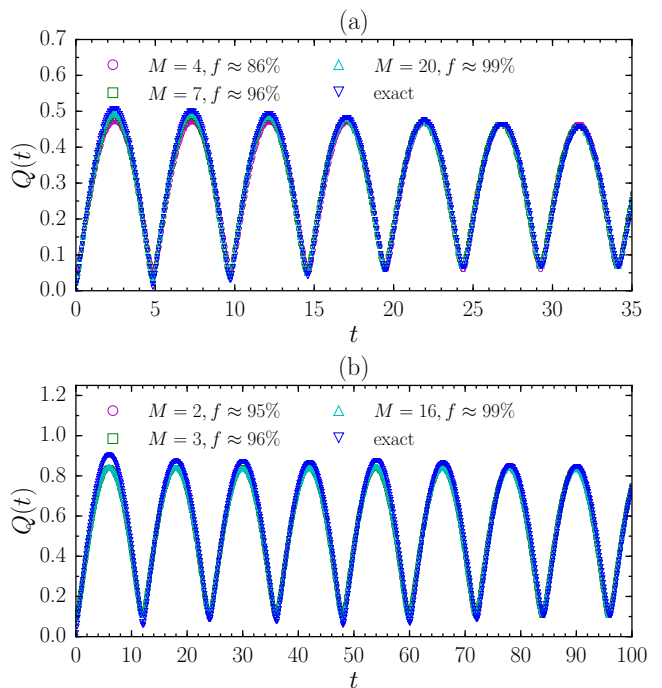


FIG. 10. Dynamics of  $Q$  projected to  $M$  eigenstates of  $H'$  with dominant  $|\langle n | \hat{V}_{0,2} | 0 \rangle|^2$ . We consider  $N = 11$  bosons at  $\nu = 1/2$  with (a) contact and (b) Coulomb interactions. The quench parameters  $A_0$  and  $A_1$  are the same as those in Figs. 4 and 5, respectively.

dynamics by a tiny spin-2 fraction of the whole Hilbert space is a compelling evidence for the picture of graviton oscillation in bimetric theory.

### Appendix C: Non-instantaneous quench

Instantaneous quench is the minimal theoretical model that describes sudden tilt of the magnetic field. However, since any experimental manipulation takes finite time, we now generalize our discussions to more realistic, non-instantaneous quenches. To be specific, we consider isotropic-anisotropic quenches driven by a time-dependent ramp of the mass tensor, i.e.,  $g_m = \text{diag}(e^{A(t)}, e^{-A(t)})$  with

$$A(t) = A_1 \exp(-t_0/t), \quad (\text{C1})$$

such that  $A(0) = 0$  and  $A(+\infty) = A_1$ . The slope of the ramp depends on some characteristic time,  $t_0$ . When  $t_0 = 0$ , we recover the instantaneous quench studied in Sec. V A. We thus expect that differences between the non-instantaneous quench and the instantaneous one are negligible when  $t_0$  is small, while some qualitative changes may happen for large enough  $t_0$ .

As a representative example, we choose  $A_1 = \ln 1.3$  (weak quench) and show the predicted behavior of  $Q$  and  $\phi$  in bimetric theory, i.e., the solutions of the full equations [Eqs. (10) and (11)], for different  $t_0$  in Fig. 11. We

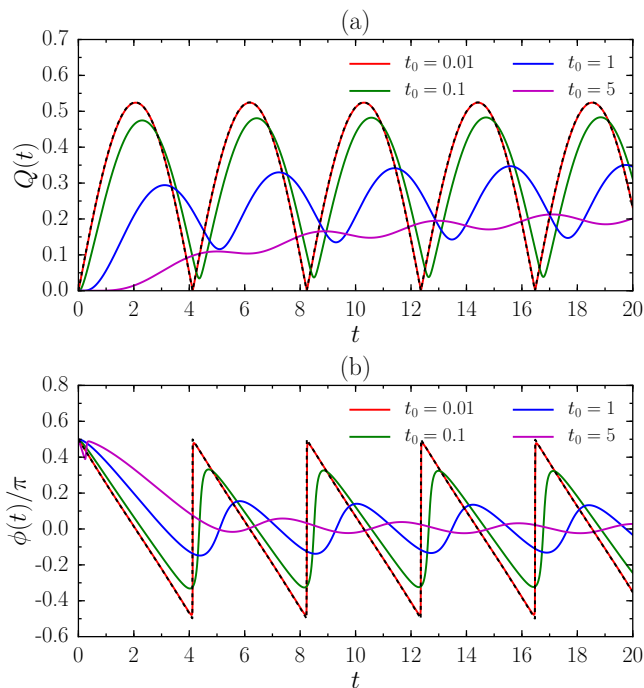


FIG. 11. Solutions of the full equations [Eqs. (10) and (11)] for the non-instantaneous quench with  $A(t) = A_1 \exp(-t_0/t)$ , under the initial condition  $Q(0) = 0$ . Here we focus on the  $Q \geq 0$  solution. We choose  $\Omega = 1.5/4$ ,  $\gamma = -1$ ,  $A_1 = \ln 1.3$ , and consider several different  $t_0 = 0.01, 0.1, 1$  and  $5$ . For comparison, we also give solutions for the instantaneous quench as black dashed lines.

indeed find that the solutions in the non-instantaneous case agree with their instantaneous limit up to  $t_0 \lesssim 10^{-2}$ . The effect of the ramp starts to appear when  $t_0 \sim 10^{-1}$ , which leads to gradual deviations of both the amplitude and frequency in the dynamics from the instantaneous case. Finally, for very large  $t_0 \gtrsim 1$ , we observe strongly distorted oscillation patterns in  $Q$  and  $\phi$ , revealing very different dynamics between the fast-quench and slow-quench regimes.

It would be interesting to compare the exact dynamics of finite systems with the predictions of bimetric theory also for non-instantaneous quenches, as what we have done for the instantaneous case in Sec. V. Due to the time-dependent nature of the non-instantaneous quench, the many-body numerical simulation in this case is more complicated and will be presented in future work. However, because the instantaneous quench corresponds to a stronger perturbation of the system, we expect similar or better agreement between theory and numerics for the case of non-instantaneous quenches.

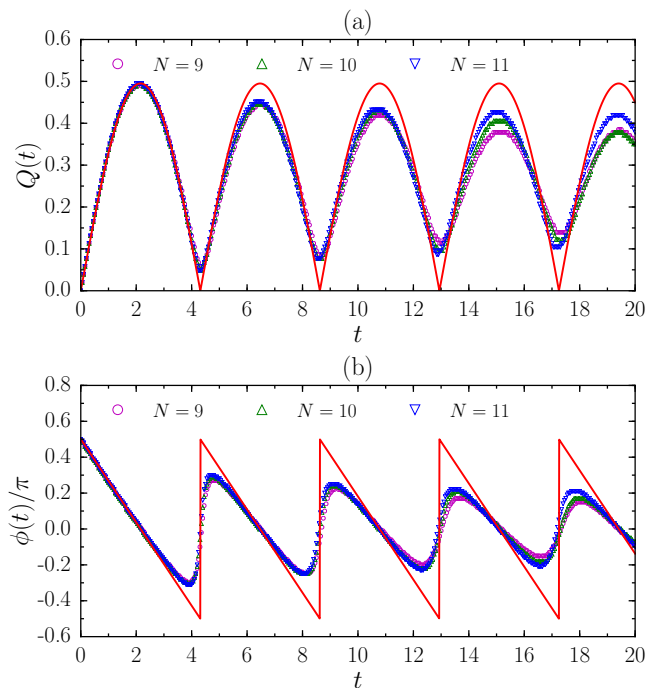


FIG. 12. Exact dynamics of (a)  $Q$  and (b)  $\phi$  for  $N = 9 - 11$  fermions at  $\nu = 1/3$  with the  $V_1$  interaction. The weak geometric quench is driven by choosing  $A_0 = 0$  and  $A_1 = \ln 1.3$ . The red solid curve is the  $Q \geq 0$  part of Eqs. (17) and (18), with  $A \approx 0.248$  and  $E_\gamma \approx 1.457$ . These two parameters are obtained by fitting the first oscillation of  $Q$  of  $N = 11$  against the solution.

#### Appendix D: Weak geometric quench for $\nu = 1/3$ fermions

Here we show the numerical results of the exact dynamics of  $\hat{g}$  for  $\nu = 1/3$  fermions and compare with the predictions of bimetric theory. As representative examples, we focus on weak isotropic-anisotropic quenches with  $A_0 = 0$  and  $A_1 > 0$ , where we choose  $A_1 = \ln 1.3$  and  $A_1 = \ln 2.0$  for quenches driven by  $V_1$  and Coulomb interactions, respectively. Exact dynamics of  $\hat{g}$  up to moderate times is shown in Figs. 12 and 13 for these two types of interactions.

Similar to  $\nu = 1/2$  bosons, the short-time dynamics of weak quenches for  $\nu = 1/3$  fermions fully agrees with bimetric theory. We can thus extract parameters  $A$  and  $E_\gamma$  by fitting the numerical data against Eqs. (17) and (18), whose values are given in the captions of Figs. 12 and 13. The value of  $A$ , which quantifies the anisotropy in the interaction, is again close to  $A_1$  (between 0 and  $A_1$ ) for the  $V_1$  (Coulomb) interaction as expected. The value of  $E_\gamma$  estimates the graviton gap as 1.46 and 0.14 for  $V_1$  and Coulomb interactions, respectively. Note that the graviton gap of the Coulomb interaction that we extract from the quench dynamics precisely matches the value given by other methods in the context of single-mode approximation [55, 63].

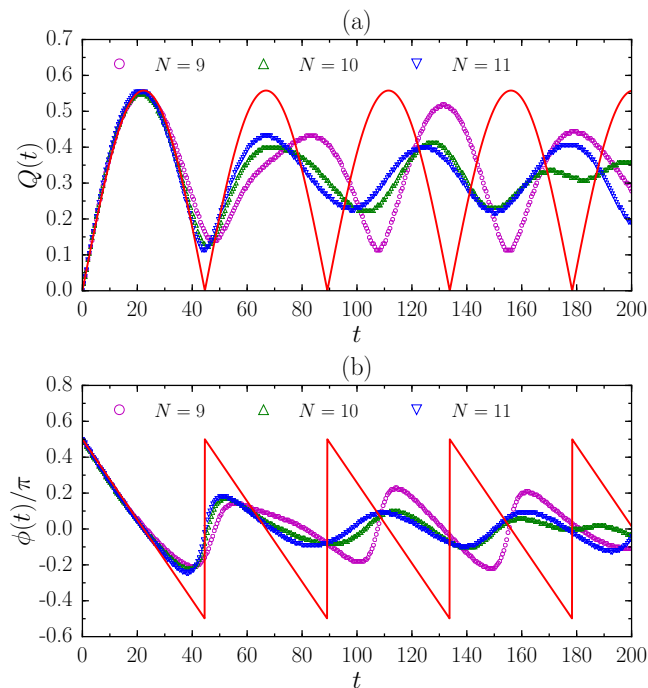


FIG. 13. Exact dynamics of (a)  $Q$  and (b)  $\phi$  for  $N = 9 - 11$  fermions at  $\nu = 1/3$  with the Coulomb interaction. The weak geometric quench is driven by choosing  $A_0 = 0$  and  $A_1 = \ln 2.0$ . The red solid curve is the  $Q \geq 0$  part of Eqs. (17) and (18), with  $A \approx 0.279$  and  $E_\gamma \approx 0.141$ . These two parameters are obtained by fitting the first oscillation of  $Q$  of  $N = 11$  against the solution.

Like in the bosonic case, we also observe deviations from bimetric theory at longer times for  $\nu = 1/3$  fermions. However, these deviations are more serious and appear earlier than those for  $\nu = 1/2$  bosons. For quenches driven by the  $V_1$  interaction, while the overall oscillation structure is maintained up to moderate times, the oscillating amplitude already obviously decays after the first oscillation (Fig. 12). The situation is even worse for quenches driven by the Coulomb interaction, as expected. In that case, the behavior of  $Q$  and  $\phi$  totally departs from simple oscillations after the first period and the curves of different system sizes are no longer on top of each other (Fig. 13). Compared with  $\nu = 1/2$  bosons, our numerical results clearly demonstrate that the dynamics of  $\nu = 1/3$  fermions suffers more from finite-size effects in the excitations and the participation of higher-spin modes.

- 
- [1] R. B. Laughlin, “Anomalous quantum hall effect: An incompressible quantum fluid with fractionally charged excitations,” *Phys. Rev. Lett.* **50**, 1395–1398 (1983).
- [2] X. G. Wen, “Topological orders in rigid states,” *Int. J. Mod. Phys. B* **04**, 239–271 (1990).
- [3] B. I. Halperin, “Quantized hall conductance, current-carrying edge states, and the existence of extended states in a two-dimensional disordered potential,” *Phys. Rev. B* **25**, 2185–2190 (1982).
- [4] X.G. Wen, “Edge excitations in the fractional quantum hall states at general filling fractions,” *Modern Physics Letters B* **05**, 39–46 (1991).
- [5] R. E. Prange and S. M. Girvin, *The Quantum Hall effect* (Springer-Verlag, 1987).
- [6] D. C. Tsui, H. L. Stormer, and A. C. Gossard, “Two-dimensional magnetotransport in the extreme quantum limit,” *Phys. Rev. Lett.* **48**, 1559–1562 (1982).
- [7] Chetan Nayak, Steven H. Simon, Ady Stern, Michael Freedman, and Sankar Das Sarma, “Non-abelian anyons and topological quantum computation,” *Rev. Mod. Phys.* **80**, 1083–1159 (2008).
- [8] J. K. Jain, “Composite-fermion approach for the fractional quantum hall effect,” *Phys. Rev. Lett.* **63**, 199–202 (1989).
- [9] Gregory Moore and Nicholas Read, “Nonabelions in the fractional quantum hall effect,” *Nuclear Physics B* **360**, 362–396 (1991).
- [10] N. Read and E. Rezayi, “Beyond paired quantum hall states: Parafermions and incompressible states in the first excited landau level,” *Phys. Rev. B* **59**, 8084–8092 (1999).
- [11] S. C. Zhang, T. H. Hansson, and S. Kivelson, “Effective-field-theory model for the fractional quantum hall effect,” *Phys. Rev. Lett.* **62**, 82–85 (1989).
- [12] X. G. Wen and A. Zee, “Shift and spin vector: New topological quantum numbers for the hall fluids,” *Phys. Rev. Lett.* **69**, 953–956 (1992).
- [13] Andrey Gromov, Gil Young Cho, Yizhi You, Alexander G. Abanov, and Eduardo Fradkin, “Framing anomaly in the effective theory of the fractional quantum hall effect,” *Phys. Rev. Lett.* **114**, 016805 (2015).
- [14] J. M. Leinaas and J. Myrheim, “On the theory of identical particles,” *Nuovo Cimento B Serie* **37**, 1–23 (1977).
- [15] F. Wilczek, “Quantum Mechanics of Fractional-Spin Particles,” *Physical Review Letters* **49**, 957–959 (1982).
- [16] X. G. Wen and A. Zee, “Classification of abelian quantum hall states and matrix formulation of topological fluids,” *Phys. Rev. B* **46**, 2290–2301 (1992).
- [17] F. D. M. Haldane and E. H. Rezayi, “Periodic laughlin-jastrow wave functions for the fractional quantized hall effect,” *Phys. Rev. B* **31**, 2529–2531 (1985).
- [18] F. D. M. Haldane and E. H. Rezayi, “Finite-size studies

- of the incompressible state of the fractionally quantized hall effect and its excitations,” *Phys. Rev. Lett.* **54**, 237–240 (1985).
- [19] J. K. Jain, *Composite Fermions* (Cambridge University Press, 2007).
- [20] Fabian H L Essler and Maurizio Fagotti, “Quench dynamics and relaxation in isolated integrable quantum spin chains,” *Journal of Statistical Mechanics: Theory and Experiment* **2016**, 064002 (2016).
- [21] Toshiya Kinoshita, Trevor Wenger, and David S. Weiss, “A quantum newton’s cradle,” *Nature* **440**, 900 (2006).
- [22] Pasquale Calabrese and John Cardy, “Quantum quenches in 1+1 dimensional conformal field theories,” *Journal of Statistical Mechanics: Theory and Experiment* **2016**, 064003 (2016).
- [23] Masahiro Nozaki, Tokiro Numasawa, and Tadashi Takayanagi, “Holographic local quenches and entanglement density,” *Journal of High Energy Physics* **2013**, 80 (2013).
- [24] F. Heidrich-Meisner, M. Rigol, A. Muramatsu, A. E. Feiguin, and E. Dagotto, “Ground-state reference systems for expanding correlated fermions in one dimension,” *Phys. Rev. A* **78**, 013620 (2008).
- [25] H. Buljan, R. Pezer, and T. Gasenzer, “Fermi-bose transformation for the time-dependent lieb-liniger gas,” *Phys. Rev. Lett.* **100**, 080406 (2008).
- [26] Jorn Mossel, Guillaume Palacios, and Jean-Sébastien Caux, “Geometric quenches in quantum integrable systems,” *Journal of Statistical Mechanics: Theory and Experiment* **2010**, L09001 (2010).
- [27] Vincenzo Alba and Fabian Heidrich-Meisner, “Entanglement spreading after a geometric quench in quantum spin chains,” *Phys. Rev. B* **90**, 075144 (2014).
- [28] J. P. Eisenstein, R. Willett, H. L. Stormer, D. C. Tsui, A. C. Gossard, and J. H. English, “Collapse of the even-denominator fractional quantum hall effect in tilted fields,” *Phys. Rev. Lett.* **61**, 997–1000 (1988).
- [29] D. Kamburov, Yang Liu, M. Shayegan, L. N. Pfeiffer, K. W. West, and K. W. Baldwin, “Composite fermions with tunable fermi contour anisotropy,” *Phys. Rev. Lett.* **110**, 206801 (2013).
- [30] J. E. Avron, R. Seiler, and P. G. Zograf, “Viscosity of quantum hall fluids,” *Phys. Rev. Lett.* **75**, 697–700 (1995).
- [31] N. Read, “Non-abelian adiabatic statistics and hall viscosity in quantum hall states and  $p_x + ip_y$  paired superfluids,” *Phys. Rev. B* **79**, 045308 (2009).
- [32] F. D. M. Haldane, ““Hall viscosity” and intrinsic metric of incompressible fractional Hall fluids,” ArXiv e-prints (2009), [arXiv:0906.1854](https://arxiv.org/abs/0906.1854) [cond-mat.str-el].
- [33] J. Maciejko, B. Hsu, S. A. Kivelson, YeJe Park, and S. L. Sondhi, “Field theory of the quantum hall nematic transition,” *Phys. Rev. B* **88**, 125137 (2013).
- [34] Yizhi You, Gil Young Cho, and Eduardo Fradkin, “Theory of nematic fractional quantum hall states,” *Phys. Rev. X* **4**, 041050 (2014).
- [35] Frank Ferrari and Semyon Klevtsov, “Fqhe on curved backgrounds, free fields and large  $n$ ,” *Journal of High Energy Physics* **2014**, 86 (2014).
- [36] Alexander G. Abanov and Andrey Gromov, “Electromagnetic and gravitational responses of two-dimensional noninteracting electrons in a background magnetic field,” *Phys. Rev. B* **90**, 014435 (2014).
- [37] Michael R. Douglas and Semyon Klevtsov, “Bergman kernel from path integral,” *Communications in Mathematical Physics* **293**, 205 (2009).
- [38] Barry Bradlyn and N. Read, “Low-energy effective theory in the bulk for transport in a topological phase,” *Phys. Rev. B* **91**, 125303 (2015).
- [39] T. Can, M. Laskin, and P. Wiegmann, “Fractional quantum hall effect in a curved space: Gravitational anomaly and electromagnetic response,” *Phys. Rev. Lett.* **113**, 046803 (2014).
- [40] S. Klevtsov and P. Wiegmann, “Geometric adiabatic transport in quantum hall states,” *Phys. Rev. Lett.* **115**, 086801 (2015).
- [41] Taylor L. Hughes, Robert G. Leigh, and Eduardo Fradkin, “Torsional response and dissipationless viscosity in topological insulators,” *Phys. Rev. Lett.* **107**, 075502 (2011).
- [42] Andrey Gromov and Alexander G. Abanov, “Density-curvature response and gravitational anomaly,” *Phys. Rev. Lett.* **113**, 266802 (2014).
- [43] F. D. M. Haldane, “Geometrical description of the fractional quantum hall effect,” *Phys. Rev. Lett.* **107**, 116801 (2011).
- [44] Andrey Gromov and Dam Thanh Son, “Bimetric theory of fractional quantum hall states,” *Phys. Rev. X* **7**, 041032 (2017).
- [45] P. Wiegmann, “Inner nonlinear waves and inelastic light scattering of fractional quantum hall states as evidence of the gravitational anomaly,” *Phys. Rev. Lett.* **120**, 086601 (2018).
- [46] F. D. M. Haldane, “Self-duality and long-wavelength behavior of the Landau-level guiding-center structure function, and the shear modulus of fractional quantum Hall fluids,” ArXiv e-prints (2011), [arXiv:1112.0990](https://arxiv.org/abs/1112.0990) [cond-mat.str-el].
- [47] Bo Yang, Zi-Xiang Hu, Z. Papić, and F. D. M. Haldane, “Model wave functions for the collective modes and the magnetoroton theory of the fractional quantum hall effect,” *Phys. Rev. Lett.* **108**, 256807 (2012).
- [48] Siavash Golkar, Dung X. Nguyen, and Dam T. Son, “Spectral sum rules and magneto-roton as emergent graviton in fractional quantum hall effect,” *Journal of High Energy Physics* **2016**, 21 (2016).
- [49] Eric A. Bergshoeff, Sjoerd de Haan, Olaf Hohm, Wout Merbis, and Paul K. Townsend, “Zwei-dreibein gravity: A two-frame-field model of 3d massive gravity,” *Phys. Rev. Lett.* **111**, 111102 (2013).
- [50] E. A. Bergshoeff, J. Rosseel, and P. K. Townsend, “On nonrelativistic 3D Spin-1 theories,” ArXiv e-prints (2018), [arXiv:1801.02527](https://arxiv.org/abs/1801.02527) [hep-th].
- [51] D. X. Nguyen, A. Gromov, and D. Thanh Son, “Fractional quantum Hall systems near nematicity: bimetric theory, composite fermions, and Dirac brackets,” ArXiv e-prints (2017), [arXiv:1712.08169](https://arxiv.org/abs/1712.08169) [cond-mat.str-el].
- [52] Bo Yang, Zi-Xiang Hu, Ching Hua Lee, and Z. Papić, “Generalized pseudopotentials for the anisotropic fractional quantum hall effect,” *Phys. Rev. Lett.* **118**, 146403 (2017).
- [53] N. R. Cooper, N. K. Wilkin, and J. M. F. Gunn, “Quantum phases of vortices in rotating bose-einstein condensates,” *Phys. Rev. Lett.* **87**, 120405 (2001).
- [54] N. Regnault and Th. Jolicoeur, “Quantum hall fractions in rotating bose-einstein condensates,” *Phys. Rev. Lett.* **91**, 030402 (2003).
- [55] S. M. Girvin, A. H. MacDonald, and P. M. Platzman,

- “Collective-excitation gap in the fractional quantum hall effect,” *Phys. Rev. Lett.* **54**, 581–583 (1985).
- [56] Bo Yang, Z. Papić, E. H. Rezayi, R. N. Bhatt, and F. D. M. Haldane, “Band mass anisotropy and the intrinsic metric of fractional quantum hall systems,” *Phys. Rev. B* **85**, 165318 (2012).
- [57] Hao Wang, Rajesh Narayanan, Xin Wan, and Fuchun Zhang, “Fractional quantum hall states in two-dimensional electron systems with anisotropic interactions,” *Phys. Rev. B* **86**, 035122 (2012).
- [58] T. Gokmen, Medini Padmanabhan, and M. Shayegan, “Transference of transport anisotropy to composite fermions,” *Nature Physics* **6**, 621 EP – (2010).
- [59] Z. Papić, “Fractional quantum hall effect in a tilted magnetic field,” *Phys. Rev. B* **87**, 245315 (2013).
- [60] Bo Yang, Ching Hua Lee, Chi Zhang, and Zi-Xiang Hu, “Anisotropic pseudopotential characterization of quantum hall systems under a tilted magnetic field,” *Phys. Rev. B* **96**, 195140 (2017).
- [61] Sonika Johri, Z Papić, P Schmitteckert, R N Bhatt, and F D M Haldane, “Probing the geometry of the Laughlin state,” *New Journal of Physics* **18**, 025011 (2016).
- [62] F Duncan M Haldane, “Fractional quantization of the hall effect—a hierarchy of incompressible quantum fluid states,” *Physical Review Letters* **51**, 605–608 (1983).
- [63] S. M. Girvin, A. H. MacDonald, and P. M. Platzman, “Magneto-roton theory of collective excitations in the fractional quantum hall effect,” *Phys. Rev. B* **33**, 2481–2494 (1986).
- [64] Cécile Repellin, Titus Neupert, Zlatko Papić, and Nicolas Regnault, “Single-mode approximation for fractional chern insulators and the fractional quantum hall effect on the torus,” *Phys. Rev. B* **90**, 045114 (2014).
- [65] Bo Yang, Zi-Xiang Hu, Z. Papić, and F. D. M. Haldane, “Model wave functions for the collective modes and the magnetoroton theory of the fractional quantum hall effect,” *Phys. Rev. Lett.* **108**, 256807 (2012).
- [66] Thierry Jolicoeur, “Shape of the magnetoroton at  $\nu = 1/3$  and  $\nu = 7/3$  in real samples,” *Phys. Rev. B* **95**, 075201 (2017).
- [67] Sean M Carroll, *Spacetime and geometry. An introduction to general relativity* (2004).
- [68] Andrey Gromov, Scott D. Geraedts, and Barry Bradlyn, “Investigating anisotropic quantum hall states with bimetric geometry,” *Phys. Rev. Lett.* **119**, 146602 (2017).
- [69] Fabio Franchini, Andrey Gromov, Manas Kulkarni, and Andrea Trombettoni, “Universal dynamics of a soliton after an interaction quench,” *Journal of Physics A: Mathematical and Theoretical* **48**, 28FT01 (2015).
- [70] F. D. M. Haldane, “Many-particle translational symmetries of two-dimensional electrons at rational Landau-level filling,” *Phys. Rev. Lett.* **55**, 2095–2098 (1985).
- [71] F. D. M. Haldane, “Fractional quantization of the hall effect: A hierarchy of incompressible quantum fluid states,” *Phys. Rev. Lett.* **51**, 605–608 (1983).
- [72] Kun Yang, “Acoustic wave absorption as a probe of dynamical geometrical response of fractional quantum hall liquids,” *Phys. Rev. B* **93**, 161302 (2016).
- [73] Elliott H. Lieb and Derek W. Robinson, “The finite group velocity of quantum spin systems,” *Comm. Math. Phys.* **28**, 251–257 (1972).
- [74] F. D. M. Haldane and Y. Shen, “Geometry of Landau orbits in the absence of rotational symmetry,” ArXiv e-prints (2015), [arXiv:1512.04502 \[cond-mat.mes-hall\]](https://arxiv.org/abs/1512.04502).
- [75] Matteo Ippoliti, Scott D. Geraedts, and R. N. Bhatt, “Composite fermions in bands with  $n$ -fold rotational symmetry,” *Phys. Rev. B* **96**, 115151 (2017).
- [76] D. Kamburov, M. A. Mueed, M. Shayegan, L. N. Pfeiffer, K. W. West, K. W. Baldwin, J. J. D. Lee, and R. Winkler, “Fermi contour anisotropy of GaAs electron-flux composite fermions in parallel magnetic fields,” *Phys. Rev. B* **89**, 085304 (2014).
- [77] M. A. Mueed, D. Kamburov, Yang Liu, M. Shayegan, L. N. Pfeiffer, K. W. West, K. W. Baldwin, and R. Winkler, “Composite fermions with a warped Fermi contour,” *Phys. Rev. Lett.* **114**, 176805 (2015).
- [78] “Multicomponent quantum hall systems: The sum of their parts and more,” in *Perspectives in Quantum Hall Effects* (Wiley-VCH Verlag GmbH, 2007) pp. 161–224.
- [79] J.P. Eisenstein, “Exciton condensation in bilayer quantum hall systems,” *Annual Review of Condensed Matter Physics* **5**, 159–181 (2014).
- [80] N. Regnault, J. Maciejko, S. A. Kivelson, and S. L. Sondhi, “Evidence of a fractional quantum hall nematic phase in a microscopic model,” *Phys. Rev. B* **96**, 035150 (2017).
- [81] Andrea Cappelli and Enrico Randellini, “Multipole expansion in the quantum hall effect,” *Journal of High Energy Physics* **2016**, 105 (2016).
- [82] R. Willett, J. P. Eisenstein, H. L. Störmer, D. C. Tsui, A. C. Gossard, and J. H. English, “Observation of an even-denominator quantum number in the fractional quantum hall effect,” *Phys. Rev. Lett.* **59**, 1776–1779 (1987).
- [83] Parsa Bonderson, Adrian E. Feiguin, and Chetan Nayak, “Numerical calculation of the neutral fermion gap at the  $\nu = 5/2$  fractional quantum hall state,” *Phys. Rev. Lett.* **106**, 186802 (2011).
- [84] Gunnar Möller, Arkadiusz Wójs, and Nigel R. Cooper, “Neutral fermion excitations in the Moore-Read state at filling factor  $\nu = 5/2$ ,” *Phys. Rev. Lett.* **107**, 036803 (2011).
- [85] Siddharth A. Parameswaran, Rahul Roy, and Shivaji L. Sondhi, “Fractional quantum hall physics in topological flat bands,” *Comptes Rendus Physique* **14**, 816 – 839 (2013).
- [86] Emil J. Bergholtz and Zhao Liu, “Topological flat band models and fractional Chern insulators,” *International Journal of Modern Physics B* **27**, 1330017 (2013).
- [87] Titus Neupert, Claudio Chamon, Thomas Iadecola, Luiz H Santos, and Christopher Mudry, “Fractional (Chern and topological) insulators,” *Physica Scripta* **2015**, 014005 (2015).
- [88] Thomas Scaffidi and Steven H. Simon, “Exact solutions of fractional Chern insulators: Interacting particles in the Hofstadter model at finite size,” *Phys. Rev. B* **90**, 115132 (2014).
- [89] Rahul Roy, “Band geometry of fractional topological insulators,” *Phys. Rev. B* **90**, 165139 (2014).
- [90] T. S. Jackson, Gunnar Möller, and Rahul Roy, “Geometric stability of topological lattice phases,” *Nature Communications* **6**, 8629 EP – (2015), article.
- [91] Fenner Harper, Steven H. Simon, and Rahul Roy, “Perturbative approach to flat Chern bands in the Hofstadter model,” *Phys. Rev. B* **90**, 075104 (2014).
- [92] Zhao Liu, Emil J. Bergholtz, Heng Fan, and Andreas M. Läuchli, “Fractional Chern insulators in topological flat bands with higher Chern number,” *Phys. Rev. Lett.* **109**,

- 186805 (2012).
- [93] Yi-Fei Wang, Hong Yao, Chang-De Gong, and D. N. Sheng, “Fractional quantum hall effect in topological flat bands with chern number two,” *Phys. Rev. B* **86**, 201101 (2012).
- [94] A. Sterdyniak, C. Repellin, B. Andrei Bernevig, and N. Regnault, “Series of abelian and non-abelian states in  $c > 1$  fractional chern insulators,” *Phys. Rev. B* **87**, 205137 (2013).
- [95] Yang-Le Wu, N. Regnault, and B. Andrei Bernevig, “Bloch model wave functions and pseudopotentials for all fractional chern insulators,” *Phys. Rev. Lett.* **110**, 106802 (2013).